PROCEEDINGS OF SCIENCE

Redefining the High-Energy gamma-ray morphology of the W51 complex with Fermi: detection of two extended components associated with W51B and W51C

Giorgio Pirola,[a,*] **Michele Peresano**[a] **and David Green**[b]

[a] *Max-Planck-Institut für Physik,*
D-85748 Garching, Germany
[b] *Cherenkov Telescope Array Observatory,*
40129 Bologna, Italy
E-mail: gpirola@mpp.mpg.de, peresano@mpp.mpg.de,
david.green@ctao-observatory.org

The W51 giant cloud is one of the largest star-forming regions (SFRs) in the Galaxy. Several experiments have detected gamma-ray emission from the W51 complex: Fermi [1], MAGIC [2], HESS [3], HAWC [4], and more recently, LHAASO [5]. This complex contains two star-forming regions, known as W51A and W51B, as well as the middle-aged supernova remnant (SNR) W51C. This last has been detected in the High-Energy (HE) gamma-ray band and is associated with the Fermi catalogue source 4FGL J1923.2+1408e. The spectral cutoff detected by LHAASO at ~400 TeV might provide the first evidence of SNRs accelerating Cosmic Rays up to PeV energies. However, LHAASO's limited angular resolution precludes a precise morphological analysis, and the two young stellar clusters contained within W51B (G48.9-0.3 and G49.2-0.3) are also valid PeVatron candidates accountable for the Ultra-High-Energy (UHE) gamma-ray emission.

We analyzed 16 years of *Fermi*-LAT data on the W51 region and found an 8σ excess, improperly fitted by the current model adopted for 4FGL J1923.2+1408e in the 4FGL catalogue. We performed a binned Likelihood analysis to identify the best-fitting model for the emitting region. We identified two overlapping extended elliptic sources, spatially coincident with the radio emission regions of W51B and W51C.

Eventually, we disentangled the HE gamma-ray emission from the W51 complex in two distinct spectral components between 1 GeV and 1 TeV: a softer LogParabola (LP) component (Γ=1.8) associated with W51C and a harder Power Law (PL) spectrum (Γ=2.4) associated with the W51B SFR. We performed a multi-wavelength modelling of the two sources, including the Very-High-Energy and UHE data from MAGIC and LHAASO. We confirmed the hadronic nature of both components. We studied the combination of two acceleration sites: the W51C old SNR shock, accelerating protons up to the TeV range, and the Super Bubbles (SB) originating from the stellar clusters contained in W51B, likely responsible for the PeV emission detected by LHAASO.

39th International Cosmic Ray Conference (ICRC2025)
15–24 July 2025
Geneva, Switzerland

*Speaker

PoS(ICRC2025)806

1. Introduction

The W51 complex ranks among the most massive and active SFRs in our Galaxy [6]. It is embedded within a giant molecular cloud (GMC) with an estimated mass of $1.2 \times 10^6 M_\odot$ and a diameter of roughly 97 pc [7]. This region hosts the middle-aged supernova remnant (SNR) W51C (G49.2-0.7), along with two major SFRs, W51A and W51B. W51C is classified as a shell-type SNR, with an estimated age of 15-30 kyr and an extended shell of $\sim 30'$ [8], corresponding to 48 pc at an assumed distance of 5.5 kpc [9].

Gamma-ray emission from W51 has been observed by several experiments, including Fermi [1], MAGIC [2], HESS [3], HAWC [4], and, more recently, LHAASO [5]. The leading explanation for the detected γ-rays is π^0 decay, produced when hadrons accelerated at the W51C shock interact with nearby molecular clouds (MCs). Support for this hadronic scenario comes from the detection of the characteristic pion bump feature [1]. LHAASO further reported emission in the 2-200 TeV range from the W51 complex, strengthening the case for W51C as a key candidate to probe the origin of Galactic cosmic rays (CRs) and test the SNR paradigm [5]. Their joint fit with Fermi-LAT data favors a hadronic origin, yielding a spectral index of 2.55 and an exponential cutoff in the proton spectrum at ~400 TeV. This picture suggests that PeV CRs may have escaped during earlier evolutionary stages and are now interacting with the MC associated with W51B. However, due to LHAASO's limited angular resolution, a detailed morphological study remains elusive, and the two young stellar clusters within W51B (G48.9-0.3 and G49.2-0.3) remain plausible PeVatron candidates responsible for the observed UHE gamma-ray emission.

2. Analysis Results

We analyzed more than 16 years of data: between August 4th, 2008 (239557417 MET) and September 30th, 2024 (749389946 MET). We started by using `fermipy`[1] v1.3.1 to reproduce W51C's known spectral energy distribution and significance maps. We fitted the model reported in the 4FGL catalog [10] for 4FGL J1923.2+1408e over a 15°-wide region of interest (ROI) centered at the source position: (290.818°, 14.145°). While the reproduced spectral energy distribution matches [1], we found an 8σ excess left, not fitted adequately by the catalogue spatial template for 4FGL J1923.2+1408e (see Fig. 1).

We investigated the hypothesis that the overall emission could be explained by two overlapping components, associated with the W51C and W51B regions. We used `gammapy`[2]-1.2, which includes asymmetric spatial radial distributions, to study the morphology of the region over 10 GeV, and we converted the best-fitting `gammapy` spatial models into templates to be used in `fermipy` to estimate the spectral energy distribution (SED) down to 1 GeV.

Regarding the morphology study, we started with the 4FGL catalog model, and we later fit three different single-source hypotheses: point source, radial Gaussian, and radial Disk. Afterwards, we added one additional PL component to the already existing LP, and compared various combinations of spatial models. The primary outcome is that a two-source scenario is significantly preferred over single-source models, and both sources exhibit a significant extension, with a 39% containment

[1] https://fermipy.readthedocs.io/en/latest/index.html
[2] https://docs.gammapy.org/1.2/

radius approximately equal to ~0.15°. In terms of significance, the first two best fitting models (2 Gaussians and a Disk and a Gaussian for W51C and W51B, respectively) are statistically equivalent, being less than 2.6σ apart. Fig. 1 shows the residual significance map obtained by adding the Disk + Gaussian morphology to the model.

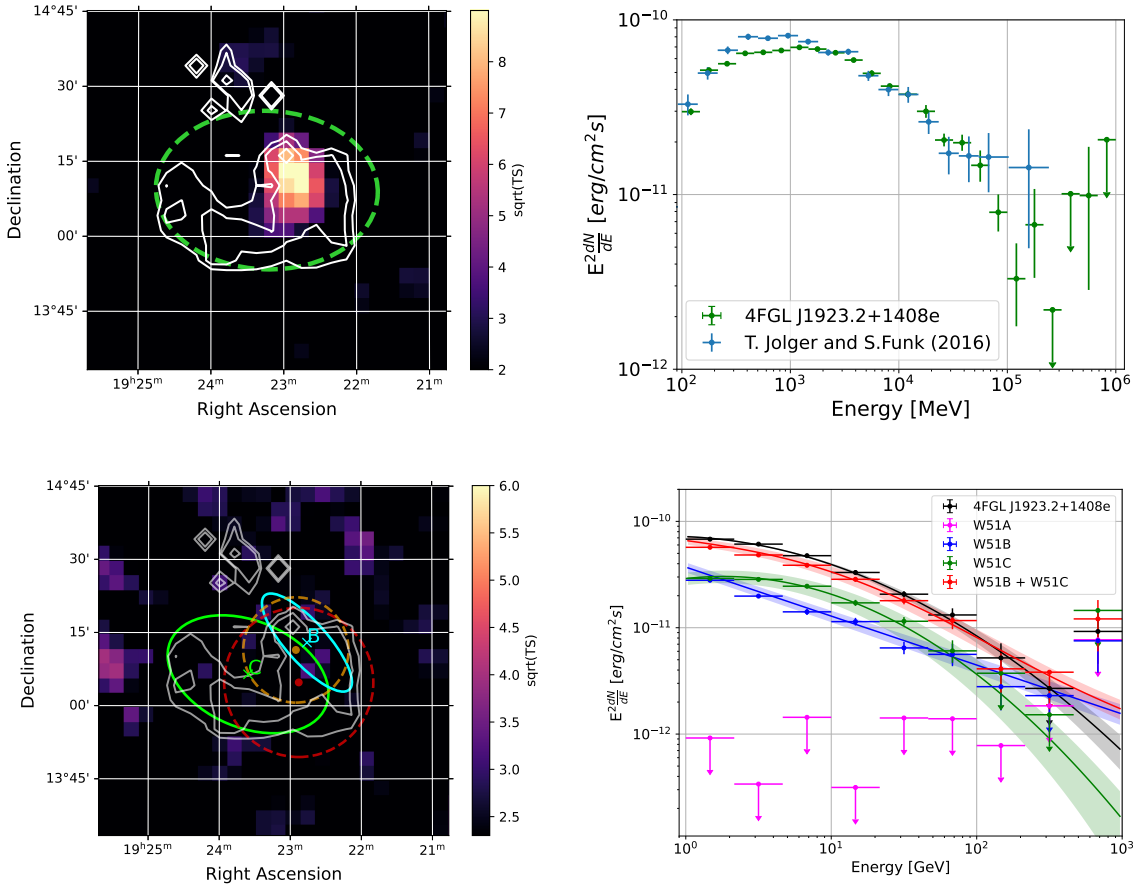

Figure 1: *Top panel*: baseline analysis between 100 MeV and 1 TeV with `fermipy`. *Left*: residual significance ($\sqrt{TS}$) map obtained by adopting the 4FGL catalog spectral model and spatial template (green dashed line) to model 4FGL J1923.2+1408e . *Right*: 4FGL J1923.2+1408e SEDs compared to the results obtained by [1]. *Bottom panel*: results obtained with best-fitting two-source model. *Left* residual significance ($\sqrt{TS}$) map above 10 GeV: the W51C disk (green) and the W51B 2D Gaussian (cyan, 68%-containment radius) are shown together with LHAASO 68%-containment radius (red), and the size of the MAGIC signal region (orange) ([5],[2]). *Right*: SEDs for the different W51 components obtained with `fermipy`. In both maps, the white radio contours are from the 1420 MHz data for the entire W51 complex [11].

We used the best-fitting spatial models to create two spatial templates to be used as `SpatialMap` objects, and we performed the spectral analysis between 1 GeV and 1 TeV with `fermipy`. We identified a softer component with a LP spectrum associated with the W51C SNR region, and a harder PL spectrum coming from the region spatially coincident with the W51B SFR (see Fig. 1). Although the differences in the integration regions between the double Gaussian scenario and the Disk + Gaussian one clearly affect the equipartition of the total emission from the region, in both cases, the spectral shape of the two components exhibits consistent features: an index value $\Gamma \sim 2.4$

for the W51B PL component, and $\alpha \sim 1.8$ and $\beta \sim 0.15$ for the LP spectrum of W51C.

3. Modeling

We discuss here a model describing two distinct non-interacting hadronic components, associated with the W51C SNR and the W51B SFR. Given the harder spectral shape of W51B and the position of the emission region detected by LHAASO, we conducted our study assuming that the gamma-ray radiation seen by LHAASO can be associated with the W51B component. On the other hand, given the absence of a more detailed energy-dependent morphology, we can assume that the emission detected below 1 TeV by MAGIC contains both contributions. Therefore, we fitted the W51C models over the Fermi-LAT points alone.

3.1 The Young Stellar Clusters in W51B

The cumulative effect of stellar winds generated by the stars contained in the cluster results in a collective wind at whose termination shock particles can be accelerated via Diffusive Shock Acceleration (DSA). We identified 3 stellar clusters within the W51B region, observed both in radio and far infrared, and spatially coincident with the gamma-ray extended emission: G48.9–0.3, G49.2.03 and G49.0.03. Two of these, G48.9–0.3 and G49.2–0.3, were addressed by [5] as potential PeVatrons responsible for the UHE gamma-ray emission.

We estimated the energetic and spatial properties of each cluster following the work of [12] and [13]. The cluster parameters are summarised in Tab. 1, where R_{TS} is the shock radius and R_b is the SB radius. For an assumed distance of 5.6 kpc [14], the density of the GMC, considering the aforementioned total mass and size, would be about 200 protons per cm^3.

Name	t_{age} [Myr]	M_c [$\cdot 10^3$ $M_\odot$]	$\dot{M}_c$ [$\cdot 10^{-5}$ $M_\odot/year$]	L_w [$\cdot 10^{37}$ erg/s]	E_{tot} [$\cdot 10^{51}$ erg]	R_{TS} [pc]	R_b [pc]
G48.9-0.3	1.10	2.40	0.71	1.78	0.62	2.09	18.01
G49.0-0.3	0.90	4.20	1.25	3.12	0.89	2.28	17.86
G49.2-0.3	0.30	7.80	2.32	5.80	0.55	1.77	10.45

Table 1: Estimated and assumed parameters for G48.9-0.3, G49.2-0.3 and G49.0-0.3, assuming a distance of 5.6 kpc [14], and environment density of 200 protons per cm^3. The estimated velocity of the shock for the three clusters is 2818 km/s. The age (t_{age}) and total mass (M_c) of the stellar clusters contained in W51B, were estimated through JHK_s-band photometric observations by [14].

Depending on the diffusion regime assumption (Kolmorov or Kraichnan), we estimated an acceleration efficiency (η_{inj}) between 11% and 15%; a compression ratio $\sigma \sim 3.4$, and a downstream to upstream diffusion coefficient ratio (D_2/D_1) between 0.1 and 0.15, for all three clusters. Finally, we also estimated the maximum proton energy (E^p_{max}) via a linear interpolation to determine the point at which the flux has been reduced of a factor e with respect to the power law extrapolation at lower energies [13]. We estimated E^p_{max} for each cluster: $263\ TeV \lesssim E^p_{max} \lesssim 398\ TeV$ and $509\ TeV \lesssim E^p_{max} \lesssim 716\ TeV$, for the Kolmogorov and Kraichnan regimes, respectively.

3.2 The W51C SNR component

We followed the work of [15] to estimate the shock velocity v_s of a middle-aged SNR interacting with a GMC. By assuming an age of 15000 years [16] and a standard total SuperNova (SN) kinetic

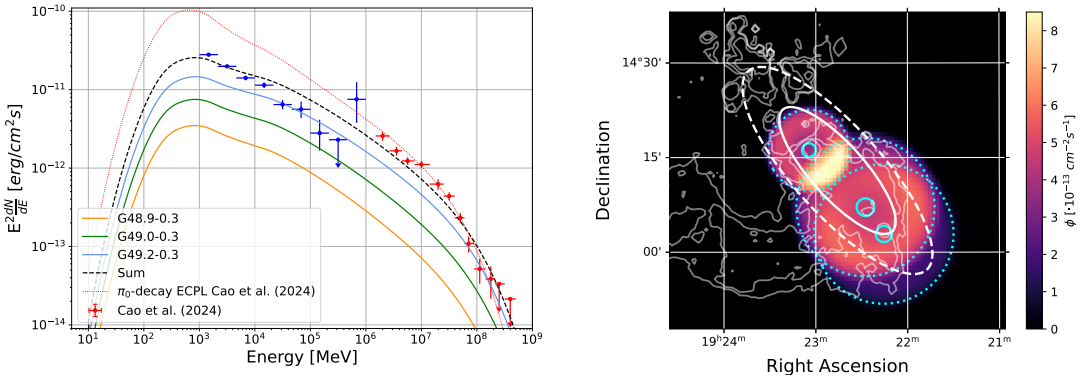

Figure 2: W51B joint fit modelling for the Kraichnan diffusive regime. *Left*: spectral fit of the Fermi-LAT (blue) and LHAASO (red) data following the model by [13]. *Right*: predicted integrated flux maps above 10 GeV. The integrated region corresponds to the area between the wind termination shock (full-line circle) and the bubble radius (dotted-line circle). The white ellipsis represents the 68% (full line) and 95% (dashed line) containment radius of Fermi-LAT 2D Gaussian. The white radio contour lines are from the THOR survey [11].

energy of 10^{51} erg, we estimated the velocity of the shock interacting with a GMG, as a function of the assumed density of the cloud and the time at which the impact with the shock occurred (see Fig. 3). From the computed shock velocity, by assuming a downstream magnetic field of $20\mu G$, we estimated the E^p_{max} achievable: 1.2 TeV $\geq E^p_{max} \geq$ 0.34 TeV for 50 $cm^{-3} \leq n_{GMC} \leq 200\ cm^{-3}$. We fitted the *Fermi*-LAT SED with an exponential-cutoff power-law (ECPL) proton distribution using `naima` [17], where the cutoff was fixed to the estimated value of the maximum energy. We found reasonable values of CR acceleration efficiency in the range of 5.4 – 9.4%, if the target particle density n_{GMC} is assumed to be 150 $cm^{-3} \leq n_{GMC} \leq 200\ cm^{-3}$.

4. Summary

By more than tripling the Fermi-LAT observation time with respect to the work done by [1], we unveiled the presence of two distinct HE gamma-ray components in the W51 complex. We identified two statistically equivalent combinations of elliptical Disk and Gaussian radial distributions that can model the emission above 10 GeV, matching the position and the extension of the W51B SFR and the W51C SNR. We resolved two spectral components down to 1 GeV: a softer LP component associated with the SNR and a harder PL describing the SFR.

We modelled the emission by probing the scenario of two independent hadronic components. We found that the three YSC contained in the W51B SFR, G48.9–0.3, G49.2.03, and G49.0.03, are suitable candidates for explaining both the HE and UHE emission. We used the model by [13] to jointly fit the Fermi-LAT and LHAASO data, and we estimated both spectral and spatial properties of the SB acceleration sites. Concerning the W51C emission, we used a standard DSA model together with the `naima` [17] package to fit the data assuming an ECPL proton distribution. The middle-aged SNR fulfills the energetic requirements to explain the HE gamma ray emission. However, the estimated size of the shock is smaller than the size of the detected gamma region,

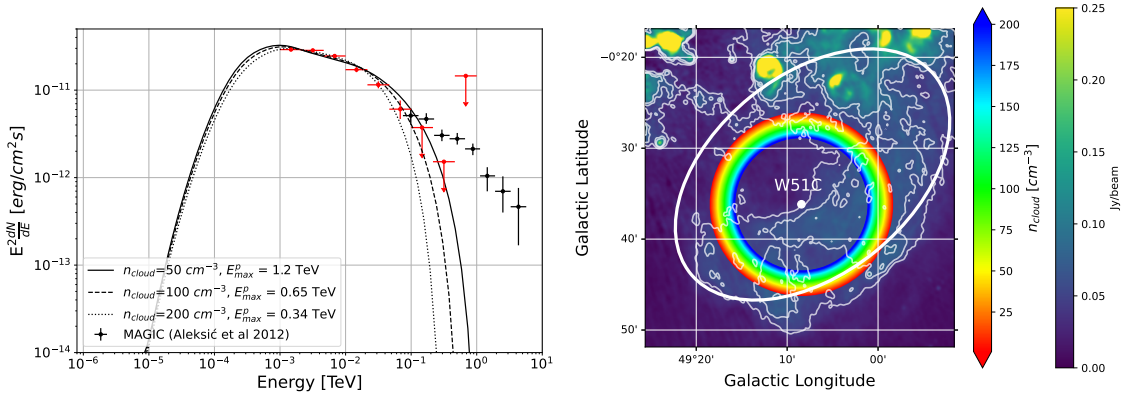

Figure 3: *Left Panel*: W51C `naima` [17] modeling fits over the Fermi-LAT data (red). The three black lines represent three different ECPL proton distributions, assuming three different values for the GMC density and consequently, three different values for the maximum proton energy. The MAGIC flux points (black) are reported as reference: they were not included in the fit. *Right Panel*: predicted extension of the SNR shock, as a function of the assumed density for the GMC (rainbow colorbar). The impact with the GMC was here simulated during the Sedov phase, corresponding to an angular shock radius of 0.10°. The white ellipsis represents the 100% containment radius of the Disk fitted over the W51C emission. The white contour line marks the radio shell from the THOR survey [11].

suggesting that the gamma-ray might be produced by CR escaping the shock and illuminating the GMC [18].

References

[1] T. Jogler and S. Funk, Revealing W51C as a Cosmic Ray Source Using Fermi-LAT Data, ApJ **816** (2016) 100.

[2] J. Aleksić, E.A. Alvarez, L.A. Antonelli, P. Antoranz, M. Asensio, M. Backes et al., Morphological and spectral properties of the W51 region measured with the MAGIC telescopes, A&A **541** (2012) A13 [1201.4074].

[3] H. E. S. S. Collaboration, H. Abdalla, A. Abramowski, F. Aharonian, F. Ait Benkhali, E.O. Angüner et al., The H.E.S.S. Galactic plane survey, A&A **612** (2018) A1 [1804.02432].

[4] A. Albert, R. Alfaro, C. Alvarez, J.R.A. Camacho, J.C. Arteaga-Velázquez, K.P. Arunbabu et al., 3HWC: The Third HAWC Catalog of Very-high-energy Gamma-Ray Sources, ApJ **905** (2020) 76 [2007.08582].

[5] Z. Cao, F. Aharonian, Axikegu, Y.X. Bai, Y.W. Bao, D. Bastieri et al., Evidence for particle acceleration approaching PeV energies in the W51 complex, Science Bulletin **69** (2024) 2833.

[6] A. Ginsburg, A review of the W51 Cloud, arXiv e-prints (2017) arXiv:1702.06627 [1702.06627].

[7] J.M. Carpenter and D.B. Sanders, The W51 Giant Molecular Cloud, AJ **116** (1998) 1856 [astro-ph/9806298].

[8] D.-S. Moon and B.-C. Koo, Thermal and Non-Thermal Radio Continuum Sources in the W51 Complex, Journal of Korean Astronomical Society **27** (1994) 81.

[9] M. Sato, M.J. Reid, A. Brunthaler and K.M. Menten, Trigonometric Parallax of W51 Main/South, ApJ **720** (2010) 1055 [1006.4218].

[10] S. Abdollahi, F. Acero, M. Ackermann, M. Ajello, W.B. Atwood, M. Axelsson et al., Fermi large area telescope fourth source catalog, The Astrophysical Journal Supplement Series **247** (2020) 33.

[11] H. Beuther, S. Bihr, M. Rugel, K. Johnston, Y. Wang, F. Walter et al., The HI/OH/recombination line survey of the inner milky way (THOR) - survey overview and data release 1, A&A **595** (2016) A32.

[12] S. Celli, A. Specovius, S. Menchiari, A. Mitchell and G. Morlino, Mass and wind luminosity of young Galactic open clusters in Gaia DR2, A&A **686** (2024) A118 [2311.09089].

[13] G. Morlino, P. Blasi, E. Peretti and P. Cristofari, Particle acceleration in winds of star clusters, MNRAS **504** (2021) 6096 [2102.09217].

[14] H.-S. Kim, Y. Nakajima, H.-K. Sung, D.-S. Moon and B.-C. Koo, A Near-Infrared Study of the Highly-Obscured Active Star-Forming Region W51B, Journal of Korean Astronomical Society **40** (2007) 17 [0704.2108].

[15] R. Yamazaki, K. Kohri, A. Bamba, T. Yoshida, T. Tsuribe and F. Takahara, TeV γ-rays from old supernova remnants, MNRAS **371** (2006) 1975 [astro-ph/0601704].

[16] B.-C. Koo and D.-S. Moon, Interaction between the W51C Supernova Remnant and a Molecular Cloud. I. H I 21 Centimeter Line Observations, ApJ **475** (1997) 194.

[17] V. Zabalza, naima: a python package for inference of relativistic particle energy distributions from observed nonthermal spectra, Proc. of International Cosmic Ray Conference 2015 (2015) 922 [1509.03319].

[18] S. Celli, G. Morlino, S. Gabici and F.A. Aharonian, Exploring particle escape in supernova remnants through gamma rays, MNRAS **490** (2019) 4317 [1906.09454].

PoS(ICRC2025)806